Journal of Power Sources Advances 35 (2025) 100186

Contents lists available at ScienceDirect

Journal of Power Sources Advances

journal homepage: www.sciencedirect.com/journal/journal-of-power-sources-advances

Novel dopamine-containing gel polymer electrolytes for Li-organic batteries

Öykü Simsek [a,b,c,d], Alessandro Innocenti [e,f], Isaac Álvarez Moisés [g], Philip Zimmer [a,b,c], Ziyuan Lyu [e,f], Simon Muench [a,b], Jean-François Gohy [g], Dominic Bresser [e,f], Ulrich S. Schubert [a,b,c,d,*]

[a] Laboratory of Organic and Macromolecular Chemistry (IOMC), Friedrich Schiller University Jena, Humboldtstraße 10, 07743, Jena, Germany
[b] Center for Energy and Environmental Chemistry Jena (CEEC Jena), Friedrich Schiller University Jena, Philosophenweg 7a, 07743, Jena, Germany
[c] Helmholtz Institute for Polymers in Energy Applications Jena (HIPOLE Jena), Lessingstrasse 12-14, 07743, Jena, Germany
[d] Helmholtz-Zentrum Berlin für Materialien und Energie, 14109, Berlin, Germany
[e] Helmholtz Institute Ulm (HIU), Helmholtzstrasse 11, 89081, Ulm, Germany
[f] Karlsruhe Institute of Technology (KIT), P.O. Box 3640, 76021, Karlsruhe, Germany
[g] Institute of Condensed Matter and Nanosciences (IMCN), Université catholique de Louvain, Place Louis Pasteur 1, Louvain-la-Neuve, 1348, Belgium

ARTICLE INFO

Keywords:
Gel polymer electrolyte
Organic batteries
UV-Induced polymerization
Electrolyte uptake
PTMA

ABSTRACT

We present a new gel polymer electrolyte (GPE) based on a dopamine-containing comonomer for lithium-organic battery cells. First, several liquid electrolyte solutions composed of an ionic liquid and a lithium salt were prepared and tested in Li-organic cells with poly(2,2,6,6-tetramethyl-1-piperidinyloxy-4-yl methacrylate) (PTMA) as the positive electrode active material to evaluate the compatibility. Among them, ionic liquid electrolyte (ILE) (1-ethyl-3-methylimidazolium bis(fluorosulfonyl)imide (EMIMFSI):lithium bis(fluorosulfonyl)imide (LiFSI), 0.8:0.2, mol:mol) was found to lead to the highest specific capacity (63.5 mAh g^{-1} at 1C). The polymer matrix composed of benzyl methacrylate (BnMA), poly(ethylene glycol) methyl ether methacrylate (mPEGMA), and dopamine methacrylamide (DMAAm) was synthesized by UV-polymerization. A literature-known polymer system without DMAAm was prepared for comparison. Samples from both polymer films were immersed in the ILE to obtain GPEs. It was found that the addition of DMAAm increased the electrolyte uptake significantly. GPEs comprising DMAAm reveal high ionic conductivity (2.3 mS cm^{-1} at 20 °C) and improved galvanostatic cycling performance in Li//PTMA cells compared to the GPEs without DMAAm.

1. Introduction

A considerable amount of research has been conducted on organic radical batteries (ORBs) due to their potential advantages like environmental friendliness, flexibility, low toxicity, and low cost [1,2]. The active materials of this system contain stable organic radicals having unpaired electrons. Galvinoxyl, hydrazyl, and nitroxyl are some examples of radical groups [3–5]. Among them, the 2,6,6,6-tetramethylpiperidinyl-*N*-oxyl (TEMPO)-moiety, a member of the nitroxyl group, has been intensively studied. Poly(2,2,6,6-tetramethylpiperidinyl-*N*-oxy methacrylate) (PTMA), having pendant TEMPO groups in each repeating unit, was presented by Nakahara et al. for the first time and has been thoroughly researched owing to high theoretical capacity of 111 mAh g^{-1}, high rate capability, and good cycling stability [6].

In most cases, these active materials are investigated in combination with commercial lithium-metal anodes, so called "Li-organic cells". In a Li//PTMA cell, during charge, the nitroxide radicals in PTMA undergo oxidation when being doped with the anions from the electrolyte, resulting in the formation of oxoammonium cations. Simultaneously, the lithium ions (Li^+) in the electrolyte are plated as metallic Li^0 on the Li anode surface. During discharge, the inverse process takes place. The one-electron redox reaction of PTMA (Fig. S1) [7] combined with the fast conduction of Li^+ and anions in the electrolyte results in good reversibility and high rate performance. Li//PTMA cells typically operate at ~3.6–3.7 V *vs.* Li^+/Li, rendering PTMA very attractive for high-power, safe, and sustainable organic battery applications.

* Corresponding author. Laboratory of Organic and Macromolecular Chemistry (IOMC), Friedrich Schiller University Jena, Humboldtstraße 10, 07743 Jena, Germany.
E-mail address: ulrich.schubert@uni-jena.de (U.S. Schubert).

https://doi.org/10.1016/j.powera.2025.100186
Received 3 April 2025; Received in revised form 31 July 2025; Accepted 16 August 2025
Available online 30 August 2025

Li-ion battery (LIB) liquid electrolytes (LEs), which are mostly lithium salts dissolved in solvents like ethylene carbonate (EC), diethyl carbonate (DEC), and/or dimethyl carbonate (DMC), are commonly utilized electrolytes in Li//PTMA cells. Although such electrolytes have high ionic conductivity greater than 10 mS cm^{-1}, they pose a safety concern because of their high volatility, flammability, and the risk of leakage [8]. In addition, the use of a separator is necessary to utilize LEs. On the contrary, ionic liquids, a class of electrolytes composed of molten salts with a melting point below 100 °C, are non-volatile and non-flammable [9,10]. Additionally, they also exhibit high ionic conductivity and feature a wide electrochemical stability window [11,12]. Moreover, lithium salts can be easily dissolved in them. However, the leakage risk and separator necessity remain in this case. Therefore, the replacement of LEs with (quasi) solid systems is crucial. Embedding ionic liquids (with lithium salts) in polymer structures results in ionic liquid-based GPEs, which not only display high ionic conductivity, but also higher flexibility compared to solid polymer electrolytes (SPEs), hence, can act as separators.

Considering the studies about GPEs for Li//PTMA cells, there is insufficient research on this topic in the literature. In 2007, Kim et al. [13] prepared fibrous poly(vinylidene fluoride-*co*-hexafluoropropylene) PVdF-HFP membranes by electrospinning and soaked them in 1 M lithium hexafluorophosphate ($LiPF_6$) in EC:DMC (1:1, vol:vol). The membranes displayed 240 % of electrolyte uptake and an ionic conductivity of 7.3×10^{-3} S cm^{-1} at 25 °C. Li/polymer electrolyte/PTMA (17 μm thickness) cells exhibited 111 mAh g^{-1} of specific capacity, while it was 68 mAh g^{-1} in the case of the cells with 36 μm-thick PTMA. Later, the authors used the same polymer matrix and immersed it in 1 M lithium bis(trifluoromethanesulfonyl)imide (LiTFSI) in 1-butyl-1-methylpyrrolidinium bis(trifluoromethylsulfonyl)imide ($Pyr_{14}TFSI$) to fabricate GPEs [14]. The cells showed 110 mAh g^{-1} of specific capacity at a rate of 1C with 99 % capacity retention between the 15th and 50th cycle. At the end of the 100th cycle at 10C, the discharge capacity was 80 mAh g^{-1} with an energy efficiency of more than 72 % with respect to the 1C-rate cycling.

Here, we propose a new GPE for Li-organic batteries based on uptake-enhancing dopamine groups. Polydopamine (PDA) has been thoroughly studied due to easy preparation, various functional groups, redox-active moieties, and outstanding adhesive properties and, therefore, plays different roles including as active electrode, electrolyte additive, coating agent for current collectors, or modification component for electrode surfaces/separators in rechargeable batteries [15–17]. Previously, the positive effect of PDA on the electrolyte affinity of separators was reported. Fang et al. stated that the electrolyte uptake of cellulose-based composite separator rose from 356 to 470 % due to the polar groups (-NH and -OH) [18]. A PDA coating on an electrospun poly (vinylidene fluoride) nanofibrous membrane caused a noteworthy change in electrolyte uptake advancing to 1160 wt% from 816 wt% owing to the hydrophilic character gained, as published by Cao et al. [19] In another work, an electrolyte uptake enhancement from 206 to 254 % was recorded for a poly(vinylidene fluoride-hexafluoropropylene) (PVDF-HFP) nonwoven-based separator after PDA coating [20]. Notwithstanding the studies on this topic, to the best of our knowledge, there has not been any work on GPEs consisting of dopamine-containing copolymers for Li-based batteries reported so far.

In this work, we developed a new GPE (GPE2) demonstrating high ionic conductivity thanks to the high electrolyte uptake provided by the polar groups of dopamine methacrylamide (DMAAm) by using ionic liquid based LE. In order to investigate the effect of DMAAm, another polymer matrix without this monomer was also synthesized (GPE1) [21]. Although mOEGMA was chosen as co-monomer for GPE1, in our work, mPEGMA was preferred. With respect to mOEGMA, mPEGMA possesses longer side chains, which boost Li^+ ions transport – an essential factor for achieving high ionic conductivity and improved electrochemical performance. These longer side chains also increase the polarity of the polymer matrix. Considering the polar nature of ILE, this helps to maintain it inside the matrix. Consequently, mPEGMA was selected over mOEGMA for the formulation of a novel polymer matrix for the gel polymer electrolyte (GPE2). For comparison, rate capability, electrochemical impedance spectroscopy (EIS), Li stripping-plating, and linear sweep voltammetry (LSV) experiments were performed for both systems. DMAAm was found to enhance the electrolyte uptake and, hence, the ionic conductivity and cycling performance. Additionally, it improves the stability of the electrolyte against Li metal according to the lower overpotential of GPE2 compared to GPE1.

2. Experimental

The monomers poly(ethylene glycol) methyl ether methacrylate 1 (mOEGMA, Mn = 300), poly(ethylene glycol) methyl ether methacrylate 2 (mPEGMA, Mn = 500), and benzyl methacrylate (BnMA) were purchased from Sigma-Aldrich. Dopamine methacrylamide (DMAAm) was purchased from Specific Polymers. The initiator benzophenone was received from Acros Organics. The inhibitors of mOEGMA, mPEGMA, and BnMA were removed by filtering them over inhibitor remover from Sigma-Aldrich. 1-Ethyl-3-methylimidazolium bis(fluorosulfonyl)imide (EMIMFSI) ionic liquid and the lithium salts lithium bis(fluorosulfonyl) imide (LiFSI), lithium bis(trifluoromethanesulfonyl) imide (LiTFSI), and lithium fluorosulfonyl(trifluoromethanesulfonyl)imide (LiFTFSI) were purchased from Proionic and Provisco, respectively. *N*-Butyl-*N*-methylpyrrolidinium bis(fluorosulfonyl) imide ($Pyr_{14}FSI$) was synthesized and purified according to the procedure reported by Montanino et al., [22–24] using *N*-methylpyrrolidone (Acros Organics) and bromobutane (Merck, 98 %) after distillation under atmospheric pressure and LiFSI after drying for 12 h at 80 °C under vacuum (10^{-3} mbar).

Before use, the two ionic liquids were dried in Büchi ovens (Glass-oven B-585) under vacuum, first at 10^{-3} mbar with a mechanical pump and then at 10^{-7} mbar with a turbo molecular pump, in both cases at room temperature for 2 h, at 50 °C for 6 h, and at 80 °C for 12 h. The lithium salts were also dried before use with the same procedure and equipment of the ionic liquids, except for LiTFSI that had a final drying temperature of 120 °C for 12 h. All drying processes were carried out in a dry room (dew point < −70 °C). All the IL-Li salt mixtures used in the study were prepared with a molar ratio of 0.8:0.2 in a dry room by dissolving the lithium salt in the ionic liquid with a magnetic stirrer. The IL-Li salt mixtures were subsequently dried again using the same procedure described for the ionic liquids. The synthesis details of PTMA with multiwalled carbon nanotubes are given in previous studies [25,26]. Briefly, 2,2,6,6-tetramethyl-4-piperidyl methacrylate and azo*bis* (isobutyronitrile) (recrystallized in ethanol) are dissolved in acetone, followed by the addition of ethylene glycol dimethacrylate (EGDME) as a cross-linking agent. After solvent removal, the precursor mixture is ball-milled (Type S1, Retsch GmbH) with multi-walled carbon nanotubes, transferred to a glass reactor, and polymerized at 80 °C in argon keeping it overnight in an oil bath. The resulting polymer mixed with carbon is extracted, washed, dried, and ball-milled. To oxidize this intermediate product, the polymer-carbon mixture is dispersed in methanol and sodium tungstate, ethylenediaminetetraacetic sodium salt, and hydrogen peroxide are added. The reaction occurs at 60 °C for 48 h, followed by filtration, washing, drying, and ball milling to obtain the final product. The weight ratio between PTMA and multi-walled carbon nanotubes is 85:15.

2.1. Fabrication of GPE1 and GPE2

GPE1 was synthesized according to a literature procedure (Fig. 1a) [21]. Briefly, BnMA and mOEGMA were mixed (3:1, mol:mol) and 0.2 wt% of benzophenone was added. This precursor was placed between two Mylar® foils and UV-induced polymerization was applied for 1 h. GPE2 was prepared by mixing BnMA, mPEGMA, and DMAAm in the ratio of 3:0.877:0.5 (mol:mol:mol) and adding 0.2 wt% of

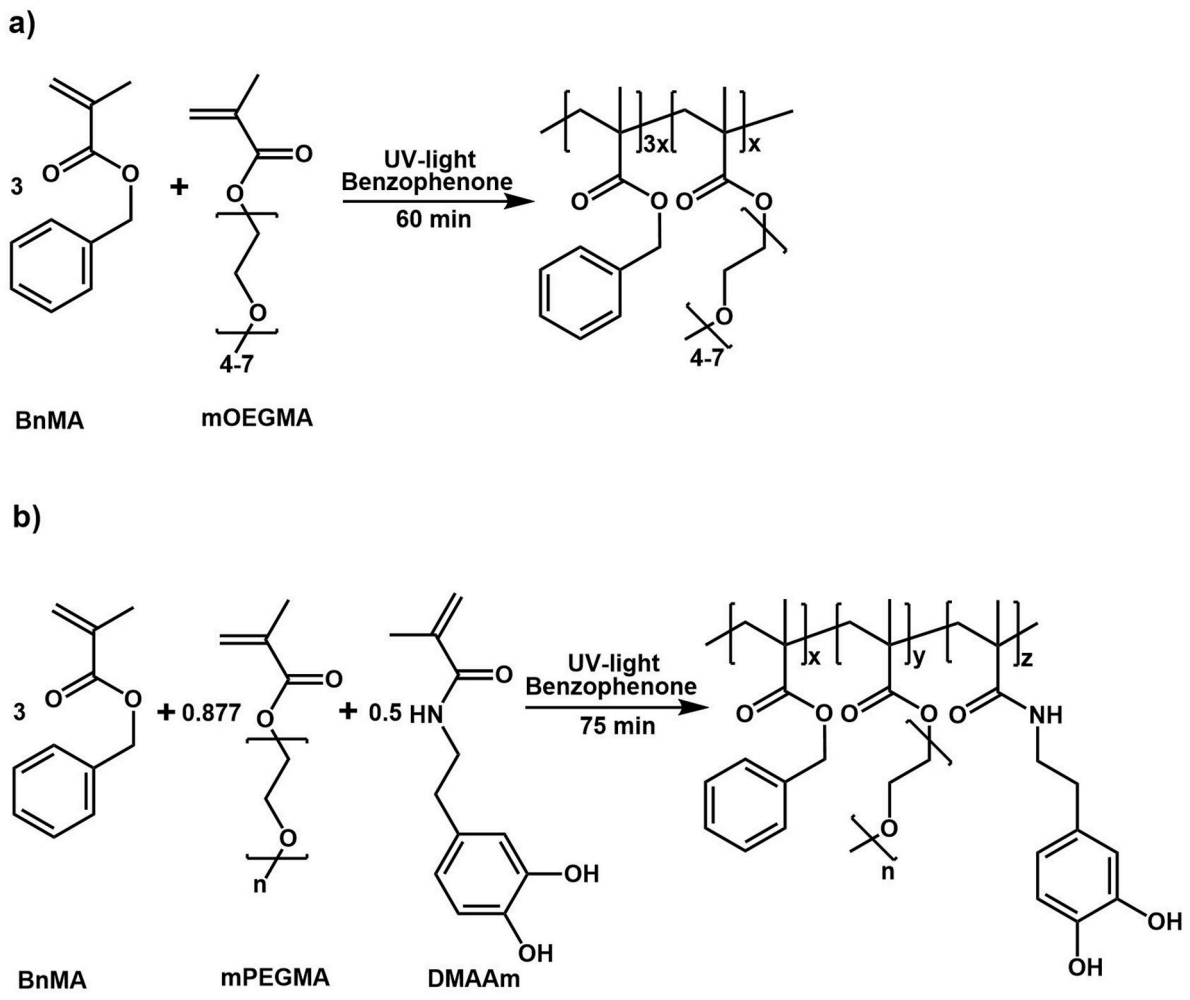

Fig. 1. Schematic representation of the polymer synthesis of a) GPE1 and b) GPE2.

benzophenone as photo-initiator (Fig. 1b). To have a homogeneous solution, the mixture was heated up 150 °C before being poured between two Mylar® foils. Thereafter, UV-irradiation was applied for 75 min in a UV-chamber (UVAcube100, Hönle). Both polymer films were placed in the ILE for 24 h. The electrolyte uptake was 117 % for GPE1 and 450 % for GPE2 (Table S1). The GPEs were prepared in the dry room.

2.2. Preparation of PTMA-MW15 cathodes

In a standard electrode preparation procedure, the following materials were combined: 900 mg of PTMA with multiwalled carbon nanotubes (Nanocyl NC700), 50 mg of conductive carbon (Super C45, IMERYS), 30 mg of carboxymethyl cellulose (CMC, Walocel CRT 2000 PPA 12) in a 3 wt% aqueous solution, 20 mg of styrene-butadiene rubber sourced from a 40 wt% latex solution (SBR, Zeon BM451-B), and 500 mg of deionized water (solid:solvent weight ratio: 40:60). To ensure thorough blending, the components underwent mixing in a planetary centrifugal mixer (ARE-250, THINKY) at 2000 rpm for 10 min. The weight ratio of the electrode components was 90:5:3:2 (PTMA:MWCNT:C45:CMC:SBR). Subsequently, the resultant mixture was cast on a carbon-coated aluminum foil (Wellcos) with a wet film thickness of 120 μm with a doctor blade. The slurry-coated foil was subsequently left to dry overnight in the dry room. Electrodes were cut with a diameter of 12 mm and pressed with a force of 1 ton. The resulting active material loading was about 4 mg cm^{-2}. These electrodes underwent further drying at 80 °C for 12 h in a Büchi oven connected to a vacuum pump, maintaining a pressure below 10^{-3} mbar. Finally, the dried electrodes were kept in the dry room.

2.3. Materials characterization

The monomer conversion of GPE2 was determined by ^{1}H NMR spectroscopy (Bruker AC 300 spectrometer, 300 MHz, DMSO-d_6), while the chemical structure was analyzed using FTIR spectroscopy (Fig. S3), X-ray diffraction (XRD) (Fig. S2), and ^{1}H NMR spectroscopy (Fig. S4). EC added at 5 mol% relative to the monomers was used as an internal standard in the precursor solution. Thereafter, this solution was UV-irradiated for 15, 45, 60, and 75 min, separately. The obtained samples were treated with DMSO-d6 overnight and passed through PTFE-filters. Afterwards ^{1}H NMR experiments were conducted. ^{1}H NMR of the monomeric precursor of GPE2 before UV-induced polymerization (300 MHz, DMSO-d6, δ in ppm): 8.65–8.76 (DMAAm OH); 7.94 (DMAAm NH); 7.27–7.42 (BnMA Ar); 6.41–6.70 (DMAAm Ar); 6.02–6.11 (mPEGMA + BnMA MA sp^2); 5.66–5.71 (mPEGMA + BnMA MA sp^2); 5.18 (BnMA Bn); 3.46–3.70 (mPEGMA EG); 3.24 (mPEGMA methoxy, DMAAm CH_2); 2.58 (DMAAm CH_2); 1.84–1.93 (mPEGMA + BnMA MA sp^3).

Thermogravimetric analysis (TGA, Netzsch TG 209F1, under nitrogen) was performed by heating from room temperature to 600 °C with a heating rate of 10 K min^{-1}.

To determine the electrochemical stability window (ESW), linear sweep voltammetry (LSV) was conducted in a voltage range from −0.5 to 5.5 V with a 1 mV s^{-1} scan rate at 20 °C using two-electrode pouch cells (ca. 2 cm^2) with nickel foil as the working electrode and lithium foil

as the counter electrode, using a VMP Biologic potentiostat/galvanostat.

Electrochemical impedance spectroscopy (EIS) was carried out on GPE1, GPE2, and ILE with stainless steel/GPE/stainless steel Swagelok cells in the frequency range of 1 MHz–10 Hz with a voltage amplitude of 20 mV at temperatures from 0 to 50 °C. In the case of ILE, a separator (GF/A, Whatman) was used. The samples were held for 2 h at each temperature before the measurement. The ionic conductivity of the different electrolytes at different temperatures was determined with EIS using RelaxIS 3 (Version 3.0.22) [27]. The EIS spectra were linearly fit to obtain the x-axes intercepts within the Nyquist plot. For this linear approach, a connection of inductor, resistor, and constant phase element in series was chosen as equivalent circuit. The resistor represents the electrolyte resistance, the constant phase element represents the dielectric behavior, and the inductor takes the inductance caused by the measurements casing and cables into account. The data range of all spectra were reduced from 4000 Hz to 200 kHz for fitting. The stability of GPEs and ILE against Li metal was evaluated with Li stripping-plating tests. Symmetric Li//Li cells (ca. 2 cm^2) with GPE/ILE were subjected to ten cycles at 0.01, 0.02, 0.05, and 0.1 mA cm^{-2} and long-term cycling at 0.02 mA cm^{-2} as the last step at 20 °C using a Maccor battery tester.

The electrochemical performances of ILE, GPE1, and GPE2 were further assessed by using Li/LE/PTMA pouch cells having glass microfiber (GF/A, Whatman) separators to employ LEs and Li/GPEs/PTMA pouch cells, both built in the dry room, and operated between 3.0 and 4.0 V for galvanostatic cycling at rates ranging from 0.1C [20] to 25C (three cycles at 0.1C, five cycles at 0.2C/0.5C/1C/2C, 50 cycles at 5C, long-term cycling at 1C) at 20 °C using a Maccor battery tester.

3. Results and discussion

3.1. Selection of the liquid electrolyte

For the purpose of determining which LE exhibits the best cell performance, they were first tested as LE without the influence of the polymer matrix. Two series of LEs were prepared for galvanostatic cell tests. EMIMFSI and $Pyr_{14}FSI$ were chosen as ionic liquids owing to their low viscosity, high ionic conductivity, broad ESW, and high solubility. Those ILs were combined with LiFSI, LiFTFSI, and LiTFSI, respectively, in a molar ratio of 0.8 to 0.2 (IL to Li-salt).

Cell tests of the LEs with $Pyr_{14}FSI$ are provided in Fig. 2a. After three formation cycles at 0.1C, the cell with LiFSI started with 34 mAh g^{-1} of discharge capacity at 0.2C. Meanwhile, this value was only 25 and 26 mAh g^{-1} in the case of the ones with LiTFSI and LiFTFSI, respectively. The cell demonstrated decreasing performance as the rate increases, and the specific capacity essentially diminished at 25C. The cell containing LiFTFSI achieved a maximum discharge capacity of 28 mAh g^{-1} at 0.2C and a very similar capacity of 27 mAh g^{-1} with LiTFSI. Differently, the cell with LiFSI attained 37 mAh g^{-1}. At 1C, the capacity of this cell decreased to 30 mAh g^{-1} and even at 5C it displayed a discharge capacity close to 20 mAh g^{-1}, while the capacities of those with LiFTFSI and LiTFSI decreased. Thus, according to the cell tests of $Pyr_{14}FSI$-based LEs, LiFSI-containing cell express better cycling behavior than that containing LiTFSI and LiFTFSI.

Regarding the LEs combining EMIMFSI and various lithium salts (Fig. 2b), the cell with LiFSI revealed higher capacity values. At 25C, however, this cell also revealed negligible capacities. Following the formation cycles, it began with 62 mAh g^{-1} of discharge capacity. In contrast to that, the ones containing LiFTFSI and LiTFSI were found to be 50 mAh g^{-1} and 49 mAh g^{-1}, individually. All cells obtained the maximum capacity at the 5th cycle at 0.2C, which was over 68 mAh g^{-1} for the one containing LiFSI. Conversely, LiFTFSI and LiTFSI displayed 59 and 57 mAh g^{-1}, respectively. The discharge capacity of the cell with LiFSI diminished to 64 mAh g^{-1} at 1C, decreasing to just below 50 mAh g^{-1} at 5C. The other cells containing LiFTFSI and LiTFSI again showed a similar behavior. Hence, also for the EMIMFSI-based electrolytes, the one comprising LiFSI revealed the best cell performance.

In summary, LiFSI achieved higher capacities compared to LiTFSI and LiFTFSI. With regard to the $Pyr_{14}FSI$ mixtures, the difference cannot be ascribed to the ionic conductivity difference between 0.2LiTFSI+0.8$Pyr_{14}FSI$ and 0.2LiFSI+0.8$Pyr_{14}FSI$, which both amount to 2.1 mS cm^{-1} at 20 °C [28,29]. Instead, it might be attributed to the fact that FSI^- anions are not only able to form a passivation film on the Al current collector and suppress the electrolytic corrosion, but also provide an improved SEI compared to $TFSI^-$ anions [30,31]. EMIMFSI illustrated much higher capacity values compared to the ones with $Pyr_{14}FSI$, which can result from the lower viscosity and accordingly higher ionic conductivity of $EMIM^+$-based ILs compared to the Pyr_{14}^+-based ILs [10]. In addition, the different cations change the polarity of the ILs and, thus, the interaction between the ILs and PTMA in the cathode. Based on the rate capability test given above, EMIMFSI-LiFSI (0.8:0.2, mol:mol) was selected to be used as swelling agent for the new GPEs and named as ionic liquid electrolyte (ILE).

3.2. Synthesis and basic characterization

In order to ascertain the impact of the ILE incorporation into P1 and P2 on their crystallinity, XRD was performed (Fig. S2). The sharper reflections of P1 and P2 detected at 18.59° and 18.30°, respectively, are compatible with 19.1° reported for poly(polyethylene glycol methyl ether)methacrylate [32]. These peaks became broader with lower density for GPE1 and GPE2, revealing that embedding an ILE significantly increases the amorphicity for both electrolytes. Notably, GPE2 is more amorphous compared to GPE1, owing to a higher content of ILE above 81 %, compared to 54 % in the case of GPE1.

For the chemical analysis of P2, FTIR was performed, and the observed peak wavenumbers were assigned to the corresponding functional groups (Fig. S3 and Table S2). To ensure high conversion of the monomers and to investigate their compatibility for copolymerization, the polymerization kinetics were examined. Based on ^1H NMR experiments, the monomer conversion during UV-polymerization was

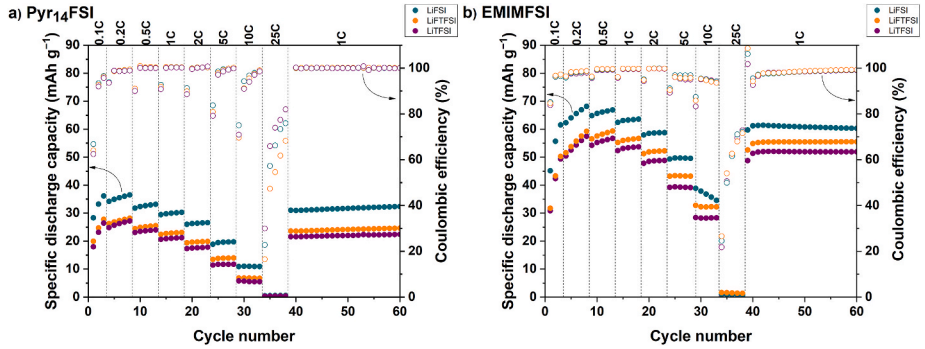

Fig. 2. Galvanostatic cycling tests of LEs based on a) $Pyr_{14}FSI$ with various lithium salts and b) EMIMFSI with various lithium salts.

calculated (Fig. S4). After 60 min, 87 % and 52 % of conversion were observed for the methacrylate-based monomers and dopamine methacrylamide, respectively, together with an incomplete film formation. During the following 15 min the conversion rate started to decrease, nevertheless, the film formation continued. Thereof, after 75 min, stable and flexible films were obtained. This is explained by a crosslinking mechanism induced by the photo-initiator benzophenone [33]. After excitation benzophenone is able to abstract a hydrogen from the side chains, leading to the formation of macroradicals that crosslink the structure by recombination [34]. Thus, 75 min were chosen as polymerization time.

It was also observed that the methacrylate-based monomers revealed a higher conversion rate and over 95 % of conversion after 75 min, while DMAAm had 67 % of conversion at the same time. It is known that methacrylamides are less reactive compared to methacrylates since they have resonance stabilization arisen from the pair of electrons on the nitrogen resulting in more stable vinyl group [35,36]. Additionally, Fugolin et al. stated that in the case of mixtures of methacrylates and methacrylamides, firstly methacrylates react and diminish the reactivity of methacrylamides [35].

The kinetics study reveals that a thorough selection of the polymerization time is important to ensure good mechanical properties of the polymer films to enable their application as separator. However, besides the mechanical properties, their thermal properties are also crucial for a safe operation of a battery. The thermal properties of the pristine polymers (polymer films before swelling) and electrolytes were determined utilizing thermogravimetric analysis (TGA) (Fig. S5). The polymer matrix of GPE1 and GPE2 before swelling were called P1 and P2. The ILE shows a high decomposition temperature (T_d) of 278 °C, which is assigned as the temperature of 5 % mass loss. This is expected since the applied ionic liquid and Li salt feature high thermal stabilities. Regarding the pristine polymers, the decomposition temperatures differ significantly with 176 °C for P1 and 265 °C for P2. This can be explained by the presence of multiple hydrogen bonds attached to DMAAm that are thought to support the thermal stability [36,37]. The GPEs, however, reveal similar thermal behavior and decomposition temperatures of 223 °C and 212 °C for GPE1 and GPE2, respectively. This reveals that the decomposition temperatures of the GPEs are primarily influenced by the ILE, because it contributes high proportions of the mass of the GPEs. Thus, all electrolytes and pristine polymers display good thermal stability for battery applications.

3.3. Electrochemical stability window

Li/GPE/Ni and Li/ILE/Ni two-electrode pouch cells were assembled to determine the ESW of the different electrolyte systems (Fig. S6). If 0.01 mA cm^{-2} is specified as oxidative stability threshold as stated by Dong et al., [38] it can be said that ILE is stable until 4.3 V *vs.* Li^+/Li, which is expected since ILs are known to commonly exhibit a broad ESW [39,40]. The decomposition of GPE2 starts at a lower potential (4.1 V) compared to the that of GPE1 (5.1 V). The earlier decomposition of GPE2 is likely explained be the fact that the -OH groups in DMAAm are thought to be oxidized at this voltage, which is in agreement with the oxidation potential of poly(dopamine) as reported by Liu et al. [41,42] Nevertheless, both ILE and GPEs are electrochemically stable between 3.0 and 4.0 V *vs.* Li^+/Li which is the voltage range applied during cell performance tests due to the cathode active material, PTMA, displaying a redox potential around 3.6 V *vs.* Li/Li^+ [43]

3.4. Ionic conductivity

Since DMAAm is a redox-active catechol containing monomer, the electrical conductivity of GPE2 was studied by EIS using a pristine polymer film. However, the electrical conductivity was found to be too low for quantification (results not shown). To determine the ionic conductivity of ILE, GPE1, and GPE2 (Fig. 3), temperature-dependent EIS was conducted. The highest ionic conductivity was obtained, as expected, for ILE amounting to 7.6 mS cm^{-1} at 20 °C, increasing to 13.0 mS cm^{-1} at 50 °C. Due to the polymer matrix not being ionically conductive, the GPEs showed lower values. Accordingly, GPE1 revealed lower ionic conductivities of 0.3 mS cm^{-1} at 20 °C and only a slight increase to 0.5 mS cm^{-1} at 50 °C.

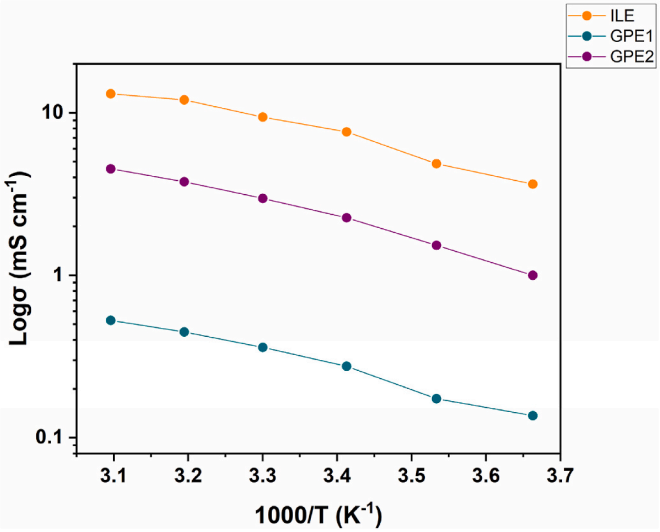

Fig. 3. Temperature dependence of the ionic conductivity of ILE, GPE1, and GPE2.

GPE2, however, achieves the ionic conductivity benchmark for practical applications (10^{-3} S cm^{-1}) [31] already at 0 °C and reaches 2.3 mS cm^{-1} at 20 °C. This dramatic difference between the GPEs can be associated with the liquid electrolyte content in the structures, which is only 54 % in GPE1, but over 81 % in GPE2. These results confirm that the improved electrolyte uptake due to DMAAm leads to much higher ionic conductivities.

3.5. Lithium stripping-plating tests

Stripping-plating tests were carried out and the obtained time-overpotential profiles are illustrated in Fig. 4. In all steps, ILE showed the lowest overpotential, which can be attributed to their highest ionic conductivity values. Higher current densities led to higher overpotentials and the initial overpotential of 4.6 mV at 0.01 mA cm^{-2} increased to 8.1 mV at 0.02 mA cm^{-2}. Similarly, it changed from 27 mV at 0.01 mA cm^{-2} to 57 mV at 0.02 mA cm^{-2} in the case of GPE1. Despite a higher overpotential, no short circuit was observed, however, the smooth shapes of GPE1 evolved sharper one and the overpotentials were not symmetrical. Additionally, the overpotential of GPE1 increased continuously and reached 157 mV after 975 cycles, which is significantly different from the 27 mV obtained at the same current density previously. Regarding GPE2, the rise in the current density from 0.01 to 0.02 mA cm^{-2} caused an overpotential increase from 13 to 27 mV. Moreover, GPE2 displayed rather stable Li stripping-plating behavior and symmetrical overpotentials ended with 34 mV even after 975 cycles. Considering all these results and previous reports, it is speculated that GPE1 has an unstable interface with the Li anode and is not able to suppress the dendrite growth [44,45]. Meanwhile, the synergistic effect of highly ionic conductive and more amorphous polymer morphology of GPE2 brought a stable interface with the Li and a good inhibition of dendrite growth, as suggested by other studies in literature [46,47].

3.6. Galvanostatic cycling tests

The electrochemical performances of ILE, GPE1, and GPE2 were further investigated by assembling pouch cells having a Li metal anode,

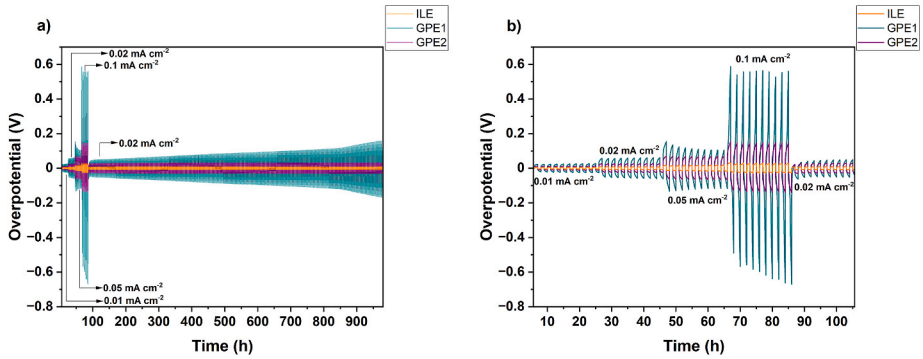

Fig. 4. Li stripping-plating test of GPE1, GPE2, and ILE at 0.01, 0.02, 0.05, 0.1, and 0.02 mA cm^{-2} a) over 900 h, b) during the first four current densities.

a PTMA cathode and GPEs/ILE as the electrolyte. In addition to the voltage profiles at 0.1C and 1C (Fig. S7), the rate capabilities were evaluated with the same protocol given in Section 2.3 as displayed in Fig. 5.

During initial cycling, increasing capacities were observed for all electrolytes, which is in accordance with other reports in the literature on PTMA, and might be assigned to an initial wetting and swelling process, resulting in more accessible/activate redox sites [14,48–50]. At the end of the formation cycles at 0.1C, the specific discharge capacity of ILE was 59 mAh g^{-1} and similarly high for GPE2 with about 56 mAh g^{-1}, while it was only 33 mAh g^{-1} for GPE1. At 0.2C, the cell with ILE and GPE2 reached maximum discharge capacities of 66 and 59 mAh g^{-1}, while it was 37 mAh g^{-1} in the case of the cell containing GPE1. At the first-applied 1C cycle, ILE exhibited 62 mAh g^{-1} of discharge capacity and GPE2 revealed a capacity of 50 mAh g^{-1}, which is twice the specific capacity provided by the GPE1 cell with 25 mAh g^{-1}. Respecting the long cycling, ILE retained its cycling performance and revealed a specific discharge capacity of about 63 mAh g^{-1}, whereas the capacity was around 43 and 19 mAh g^{-1} in the case of GPE2 and GPE1, respectively.

It can be explained by having higher ionic conductivity ensuring faster Li^+ diffusion with an enhanced battery performance. The cell employing GPE2 kept 35.4 % of its capacity after 500 cycles and ended with 15 mAh g^{-1}. Considering the DMAAm conversion, which is less than 70 %, the unpolymerized monomers may have a negative influence on the capacity retention by causing detrimental side reactions. The cell containing GPE1 lost almost 80 % of its capacity resulting in only ca. 4 mAh g^{-1} at the end of 500 cycles. Moreover, although GPE2 demonstrates an oxidation onset approaching 4.1 V, nearly coinciding with the 4.0 V anodic cut-off, the good electrochemical stability of GPE2 is attributed to the presence of catechol groups in the DMAAm units. These groups impart antioxidant behavior and radical-scavenging capabilities, effectively mitigating oxidative degradation [51]. They have been extensively shown to function as strong antioxidants by donating a hydrogen atom from one of their hydroxyl (–OH) groups to a free radical resulting in the formation of a semiquinone radicals or quinones [52,53]. Subsequently, the semiquinone radical intermediate can engage with an additional free radical, thereby further mitigating oxidative degradation [54]. Possibly, this multi-step antioxidant cascade plays a critical role in fortifying the electrode-electrolyte interface, promoting enhanced electrochemical stability and longevity of the system. Furthermore, as Lee et al. [55] reported, a polydopamine-containing passivation layer might be formed on the cathode surface during the precycling step, thereby suppressing the decomposition of the electrolyte.

Despite ILE exhibiting better cell performance in general, it still requires the use of a separator and carries the leakage risk which poses a safety concern. Besides, GPE2 was found to show rather similar capacity values to that of ILE at lower C-rates. In comparison with GPE1, the dopamine groups of GPE2 improved the electrolyte uptake due to the polar groups and, hence, also ionic conductivity bringing to a better electrochemical performance in addition to more stable cycling behavior.

4. Conclusion

In summary, we reported a new GPE for Li//PTMA cells comprising dopamine groups increasing the electrolyte uptake significantly and exhibiting a high ionic conductivity of 2.3 mS cm^{-1} at 20 °C. Methacrylate-based and dopamine-containing comonomers were combined with benzophenone and UV-polymerized for 75 min. The fabricated polymer films were immersed in the liquid electrolyte composed of LiFSI and EMIMFSI. The obtained GPEs reveal 450 % of electrolyte uptake with a wide electrochemical stability window (over 4 V), low and stable overpotentials (34 mV at 0.02 mA cm^{-2} even after 975 h at 20 °C). The Li//PTMA cell utilizing this GPE2 obtained 59 mAh g^{-1} of maximum discharge capacity at 0.2C. GPEs without dopamine groups were synthesized for comparison according to literature and demonstrated only 117 % of electrolyte uptake with, accordingly, much lower

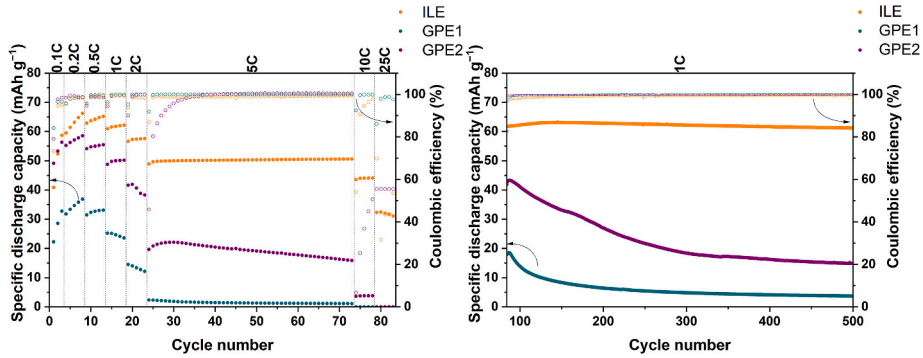

Fig. 5. Galvanostatic cycling tests of ILE, GPE1, as well as GPE2 at a) during rate capability test and b) during long cycling.

ionic conductivity. Therefore, they achieved 37 mAh g^{-1} of maximum discharge capacity at 0.2C and revealed quite high and unstable overpotential (157 mV after 975 h at 20 °C) during stripping-plating tests. In summary, dopamine groups provided an enhanced electrolyte uptake and improved electrochemical properties in GPEs, therefore, constituting a promising electrolyte system for Li-organic batteries.

CRediT authorship contribution statement

Öykü Simsek: Writing – original draft, Visualization, Validation, Methodology, Investigation, Formal analysis, Data curation, Conceptualization. **Alessandro Innocenti:** Writing – review & editing, Methodology, Investigation, Data curation, Conceptualization. **Isaac Álvarez Moisés:** Resources. **Philip Zimmer:** Formal analysis. **Ziyuan Lyu:** Resources. **Simon Muench:** Writing – review & editing, Supervision. **Jean-François Gohy:** Writing – review & editing, Supervision. **Dominic Bresser:** Writing – review & editing, Supervision. **Ulrich S. Schubert:** Writing – review & editing, Supervision, Funding acquisition.

Declaration of competing interest

The authors declare that they have no known competing financial interests or personal relationships that could have appeared to influence the work reported in this paper.

Acknowledgement

The authors would like to acknowledge the financial support from the European Union's Horizon 2020 research and innovation program under the Marie Skłodowska-Curie grant agreement No 860403. The authors further thank Dominik Steinle and Dr. Grégoire Vansse for their useful comments and fruitful discussions.

Appendix A. Supplementary data

Supplementary data to this article can be found online at https://doi.org/10.1016/j.powera.2025.100186.

Data availability

Data will be made available on request.

References

[1] C. Friebe, U.S. Schubert, High-power-density Organic Radical Batteries, Springer Nature, 2019.
[2] K.-A. Hansen, J. Nerkar, K. Thomas, S.E. Bottle, A.P. O'Mullane, P.C. Talbot, J. P. Blinco, ACS Appl. Mater. Interfaces 10 (2018) 7982–7988.
[3] P. Ionita, B. Gilbert, A. Whitwood, Lett. Org. Chem. 1 (2004) 70–74.
[4] G.M. Coppinger, J. Am. Chem. Soc. 79 (1957) 501–502.
[5] V.V. Khramtsov, A.A. Bobko, M. Tseytlin, B. Driesschaert, Anal. Chem. 89 (2017) 4758–4771.
[6] K. Nakahara, S. Iwasa, M. Satoh, Y. Morioka, J. Iriyama, M. Suguro, E. Hasegawa, Chem. Phys. Lett. 359 (2002) 351–354.
[7] S. Wang, F. Li, A.D. Easley, J.L. Lutkenhaus, Nat. Mater. 18 (2019) 69–75.
[8] J. Kalhoff, G.G. Eshetu, D. Bresser, S. Passerini, ChemSusChem 8 (2015) 2154–2175.
[9] A. Balducci, Ionic Liquids in Lithium-Ion Batteries, Springer Nature, 2018.
[10] X. Liu, A. Mariani, H. Adenusi, S. Passerini, Angew. Chem. Int. Ed. 62 (2023) e202219318.
[11] X. Tang, S. Lv, K. Jiang, G. Zhou, X. Liu, J. Power Sources 542 (2022) 231792.
[12] D. Bresser, S. Passerini, B. Scrosati, Chem. Commun. 49 (2013) 10545–10562.
[13] J.-K. Kim, G. Cheruvally, J.-W. Choi, J.-H. Ahn, D.S. Choi, C.E. Song, J. Electrochem. Soc. 154 (2007) A839.
[14] J.-K. Kim, A. Matic, J.-H. Ahn, P. Jacobsson, RSC Adv. 2 (2012) 9795–9797.
[15] H. Li, D. Yin, W. Li, Q. Tang, L. Zou, Q. Peng, Colloids Surf. B Biointerfaces 199 (2021) 111502.
[16] S. Fan, W. Lin, Y. Huang, J. Xia, J.-F. Xu, J. Zhang, J. Pi, Front. Pharmacol. 13 (2022) 829712.
[17] H. Khezraqa, S.-A. Safavi-Mirmahalleh, H. Roghani-Mamaqani, M. Salami-Kalajahi, J. Energy Storage 79 (2024) 110170.
[18] Y. Fang, Z. Zhang, S. Liu, Y. Pei, X. Luo, Electrochim. Acta 475 (2024) 143661.
[19] C. Cao, L. Tan, W. Liu, J. Ma, L. Li, J. Power Sources 248 (2014) 224–229.
[20] C. Shi, J. Dai, S. Huang, C. Li, X. Shen, P. Zhang, D. Wu, D. Sun, J. Zhao, J. Membr. Sci. 518 (2016) 168–177.
[21] P. Isken, M. Winter, S. Passerini, A. Lex-Balducci, J. Power Sources 225 (2013) 157–162.
[22] M. De Francesco, E. Simonetti, G. Gorgi, G.B. Appetecchi, Challenges 8 (2017) 11.
[23] M. Montanino, F. Alessandrini, S. Passerini, G.B. Appetecchi, Electrochim. Acta 96 (2013) 124–133.
[24] A. Balducci, S. Jeong, G. Kim, S. Passerini, M. Winter, M. Schmuck, G. Appetecchi, R. Marcilla, D. Mecerreyes, V. Barsukov, J. Power Sources 196 (2011) 9719–9730.
[25] A. Vlad, J. Rolland, G. Hauffman, B. Ernould, J.F. Gohy, ChemSusChem 8 (2015) 1692–1696.
[26] A. Innocenti, I.Á. Moisés, O. Lužanin, J. Bitenc, J.-F. Gohy, S. Passerini, ACS Appl. Mater. Interfaces (2023).
[27] P. Adeli, J.D. Bazak, K.H. Park, I. Kochetkov, A. Huq, G.R. Goward, L.F. Nazar, Angew. Chem. Int. Ed. 58 (2019) 8681–8686.
[28] E. Paillard, Q. Zhou, W.A. Henderson, G.B. Appetecchi, M. Montanino, S. Passerini, J. Electrochem. Soc. 156 (2009) A891.
[29] F. Wu, G.T. Kim, T. Diemant, M. Kuenzel, A.R. Schür, X. Gao, B. Qin, D. Alwast, Z. Jusys, R.J. Behm, Adv. Energy Mater. 10 (2020) 2001830.
[30] I.A. Shkrob, T.W. Marin, Y. Zhu, D.P. Abraham, J. Phys. Chem. C 118 (2014) 19661–19671.
[31] G.A. Elia, U. Ulissi, S. Jeong, S. Passerini, J. Hassoun, Energy Environ. Sci. 9 (2016) 3210–3220.
[32] P. Khomein, A. Nallapaneni, J. Lau, D. Lilley, C. Zhu, S. Kaur, R. Prasher, G. Liu, Sol. Energy Mater. Sol. Cell. 225 (2021) 111030.
[33] M. Doytcheva, R. Stamenova, V. Zvetkov, C.B. Tsvetanov, Polymer 39 (1998) 6715–6721.
[34] B. Rupp, M. Schmuck, A. Balducci, M. Winter, W. Kern, Eur. Polym. J. 44 (2008) 2986–2990.
[35] A.P. Fugolin, S. Lewis, M.G. Logan, J.L. Ferracane, C.S. Pfeifer, Dent. Mater. 36 (2020) 1028–1037.
[36] L. Barcelos, M. Borges, C. Soares, M. Menezes, V. Huynh, M. Logan, A. Fugolin, C. Pfeifer, Dent. Mater. 36 (2020) 468–477.
[37] W. Hu, S. Lu, Z. Zhang, L. Zhu, Y. Wen, T. Zhang, Z. Ji, Biomater. Sci. 7 (2019) 1323–1334.
[38] X. Dong, A. Mayer, X. Liu, S. Passerini, D. Bresser, ACS Energy Lett. 8 (2023) 1114–1121.
[39] E. Kim, J. Han, S. Ryu, Y. Choi, J. Yoo, Materials 14 (2021) 4000.
[40] A. Lewandowski, A. Świderska-Mocek, J. Power Sources 194 (2009) 601–609.
[41] X. Yang, M. Jiang, X. Gao, D. Bao, Q. Sun, N. Holmes, H. Duan, S. Mukherjee, K. Adair, C. Zhao, Energy Environ. Sci. 13 (2020) 1318–1325.
[42] T. Liu, K.C. Kim, B. Lee, Z. Chen, S. Noda, S.S. Jang, S.W. Lee, Energy Environ. Sci. 10 (2017) 205–215.
[43] H. Nishide, Green Chem. 24 (2022) 4650–4679.
[44] K. Deng, J. Qin, S. Wang, S. Ren, D. Han, M. Xiao, Y. Meng, Small 14 (2018) 1801420.
[45] L. Li, M. Wang, J. Wang, F. Ye, S. Wang, Y. Xu, J. Liu, G. Xu, Y. Zhang, Y. Zhang, J. Mater. Chem. A 8 (2020) 8033–8040.
[46] P. Zhai, W. He, C. Zeng, L. Li, W. Yang, Chem. Eng. J. 451 (2023) 138414.
[47] S. Li, W. Ren, Y. Huang, Q. Zhou, C. Luo, Z. Li, X. Li, M. Wang, H. Cao, Electrochim. Acta 391 (2021) 138950.
[48] M. Uhl, T. Geng, P.A. Schuster, B.W. Schick, M. Kruck, A. Fuoss, A.J. Kuehne, T. Jacob, Angew. Chem. Int. Ed. 62 (2023) e202214927.
[49] X.-H. Chen, H. Lu, Z. Wu, H. Wang, S. Zhang, S. Mei, G. Long, Q. Zhang, C.-J. Yao, J. Mater. Chem. A 11 (2023) 77–83.
[50] M. Uhl, Sadeeda, P. Penert, P.A. Schuster, B.W. Schick, S. Muench, A. Farkas, U. S. Schubert, B. Esser, A.J. Kuehne, ChemSusChem 17 (2024) e202301057.
[51] S. Zafar, R. Ahmed, R. Khan, Free Radic. Res. 50 (2016) 939–948.
[52] A.C. Gómez-Herrero, C. Sánchez-Sánchez, F. Chérioux, J.I. Martínez, J. Abad, L. Floreano, A. Verdini, A. Cossaro, E. Mazaleyrat, V. Guisset, Chem. Sci. 12 (2021) 2257–2267.
[53] N. Schweigert, A.J. Zehnder, R.I. Eggen, Environ. Microbiol. 3 (2001) 81–91.
[54] L. Valgimigli, R. Amorati, M.G. Fumo, G.A. DiLabio, G.F. Pedulli, K.U. Ingold, D. A. Pratt, J. Org. Chem. 73 (2008) 1830–1841.
[55] H. Lee, T. Han, K.Y. Cho, M.-H. Ryou, Y.M. Lee, ACS Appl. Mater. Interfaces 8 (2016) 21366–21372.